LETTERS
PUBLISHED ONLINE: 14 DECEMBER 2008 | DOI: 10.1038/NPHYS1155
nature physics

# Attosecond phase locking of harmonics emitted from laser-produced plasmas

Y. Nomura[1]*, R. Hörlein[1,2]*, P. Tzallas[3], B. Dromey[4], S. Rykovanov[1,5], Zs. Major[1], J. Osterhoff[1], S. Karsch[1], L. Veisz[1], M. Zepf[4], D. Charalambidis[3,6], F. Krausz[1,2] and G. D. Tsakiris[1]†

**Laser-driven coherent extreme-ultraviolet (XUV) sources provide pulses lasting a few hundred attoseconds[1,2], enabling real-time access to dynamic changes of the electronic structure of matter[3,4], the fastest processes outside the atomic nucleus. These pulses, however, are typically rather weak. Exploiting the ultrahigh brilliance of accelerator-based XUV sources[5] and the unique time structure of their laser-based counterparts would open intriguing opportunities in ultrafast X-ray and high-field science, extending powerful nonlinear optical and pump–probe techniques towards X-ray frequencies, and paving the way towards unequalled radiation intensities. Relativistic laser–plasma interactions have been identified as a promising approach to achieve this goal[6–13]. Recent experiments confirmed that relativistically driven overdense plasmas are able to convert infrared laser light into harmonic XUV radiation with unparalleled efficiency, and demonstrated the scalability of the generation technique towards hard X-rays[14–19]. Here we show that the phases of the XUV harmonics emanating from the interaction processes are synchronized, and therefore enable attosecond temporal bunching. Along with the previous findings concerning energy conversion and recent advances in high-power laser technology, our experiment demonstrates the feasibility of confining unprecedented amounts of light energy to within less than one femtosecond.**

The nonlinear response of matter exposed to intense femtosecond laser pulses gives rise to the emission of high-frequency radiation at harmonics of the laser oscillation frequency. If the harmonics are phase-locked, their superposition results in a train of attosecond bursts[20]. The concept has been so far successfully implemented in atomic gases[21], and culminated in isolated attosecond pulses by using few-cycle laser drivers[1,2]. The low generation efficiency of harmonic radiation from atoms has motivated research into alternative concepts. Dense, femtosecond-laser-produced plasmas hold promise of converting laser light into coherent harmonics with much higher efficiency and of exploiting much higher laser intensities, because the plasma medium—in contrast to the atomic emitters—imposes no restriction on the strength of the laser field driving the harmonics[6–13]. Recent experimental studies of harmonics produced from overdense plasmas impressively corroborate several theoretical predictions: the high conversion efficiency[19], the favourable scalability of the generation technique towards high photon energies[14,16,19] and excellent divergence due to the spatial coherence of the generated harmonics[19,22]. Whether the high-order harmonics that are produced in overdense plasmas possess the phase synchronism necessary for attosecond bunching of the produced radiation has lacked experimental evidence up to now. In this work we demonstrate that this is indeed the case and hence the door is open for the generation of attosecond XUV pulses many orders of magnitude more intense than available at present.

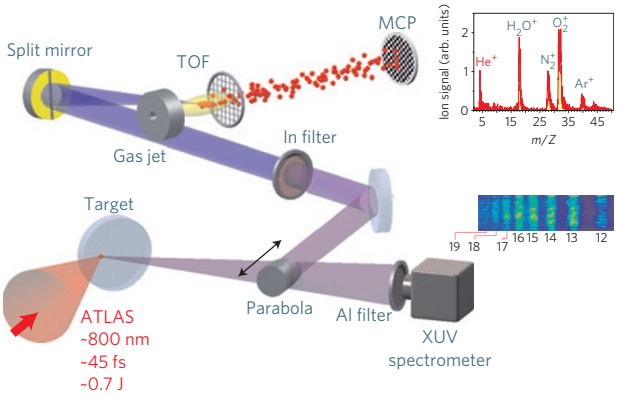


**Figure 1 | Schematic diagram of the experimental set-up for the harmonic generation and its temporal characterization.** The light reflected off the target into the specular direction is recollimated by a 25.4-mm-diameter 90° gold-coated off-axis parabolic mirror with the same focal length as the laser focusing parabola. The recollimating mirror is mounted on a flipper stage for easy withdrawal, thus enabling the spectral characterization of the emitted XUV light. Thin metal filters (typically 150 nm Al, In or Sn) inserted in front of the spectrometer provide a spectral preselection and block the laser light. With the recollimating parabolic mirror in place, the beam is deflected towards a 120-mm-diameter glass plate positioned at 60° angle of incidence. The reflection off the glass plate close to Brewster's angle (~57°) suppresses the *p*-polarized infrared laser light while reflecting a substantial fraction (~5% in *p* polarization) of the XUV harmonic emission. The 150 nm In filter selects harmonics from H8 to H14 and suppresses the residual laser light. This harmonic composition is focused into the He jet by a 300-mm-radius-of-curvature spherical mirror split into two halves, serving as a focusing wavefront divider. The generated ions are detected using a time-of-flight (TOF) spectrometer and a multichannel-plate (MCP) detector. The insets show raw data of a typical mass (upper) and harmonic (lower) spectrum.

Efficient harmonic generation from laser-produced plasmas relies on field strengths that result in values of the vector potential $a_L = |e|A_L/mc = \sqrt{I_L\lambda_L^2/(1.37\times10^{18}\,\mathrm{W\,\mu m^2\,cm^{-2}})}$ close

[1]Max-Planck-Institut für Quantenoptik, Hans-Kopfermann-Straße 1, D-85748 Garching, Germany, [2]Department für Physik, Ludwig-Maximilians-Universität, Am Coulombwall 1, D-85748 Garching, Germany, [3]Foundation for Research and Technology-Hellas, Institute of Electronic Structure & Laser, PO Box 1527, GR-711 10 Heraklion (Crete), Greece, [4]Department of Physics and Astronomy, Queens University Belfast, BT7 1NN, UK, [5]Moscow Physics Engineering Institute, Kashirskoe shosse 31, 115409 Moscow, Russia, [6]Department of Physics, University of Crete, PO Box 2208, GR-71003 Voutes-Heraklion (Crete), Greece. *These authors contributed equally to this work. †e-mail: george.tsakiris@mpq.mpg.de.

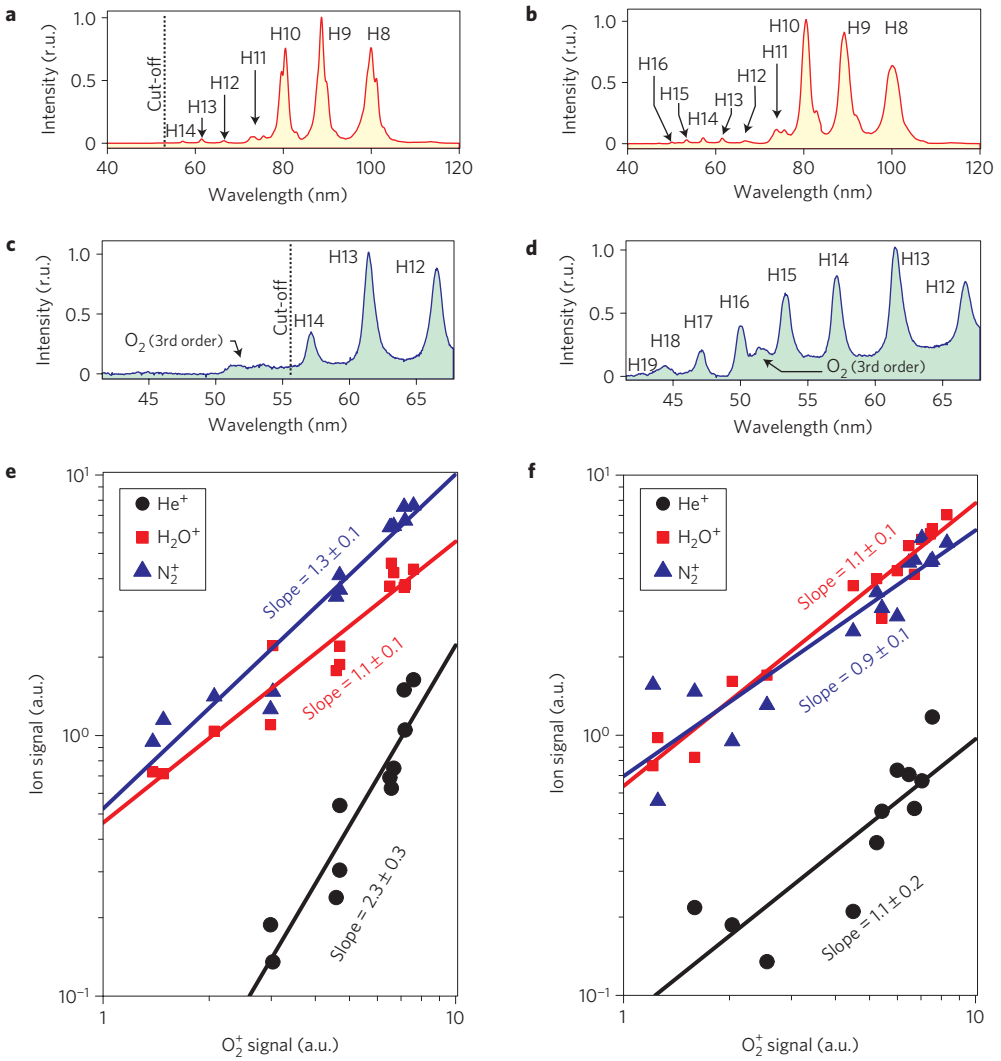


**Figure 2 | Outline of the harmonic spectra and ion-yield dependence on the XUV radiation intensity for two target materials. a**,**c**,**e**, Low-density (PMMA density ~1.2 g cm$^{-3}$) target; **b**,**d**,**f**, high density (glass density ~2.6 g cm$^{-3}$) target. The spectra shown in **a** and **b** have been filtered with a 150 nm In filter, whereas those in **c** and **d** with a 150 nm Al filter transmitting all harmonics above H10. In these panels a spurious signal due to third-order diffraction of $O_2$ line emission (~17 nm) is visible. As seen in **a** and **c**, the low-density target clearly shows the high-frequency cut-off at H14. By contrast, the spectrum in **d**, from the high-density target taken with the Al filter, extends to H19. **e**,**f**, The corresponding ion yields of various species (including those from the background gas) due to the harmonic composition shown in **a** and **b** against the $O_2^+$ yield. The dependence with slope ~1 indicates single-photon ionization whereas that with slope ~2 is evidence of two-photon ionization. The $O_2^+$ signal is proportional to the total XUV pulse energy because it is ionized by a single photon of any harmonic in the composition.

to (or larger than) unity. Here $e$ and $m$ are the electron's charge and rest mass, respectively, $c$ is the velocity of light and $A_L$, $I_L$ and $\lambda_L$ stand for the amplitude of the vector potential, the cycle-averaged intensity and the wavelength of the incident laser light. Two distinct mechanisms have been identified to give rise to XUV harmonic emission from overdense plasmas produced by femtosecond laser pulses incident on a solid surface. One is based on a relativistic Doppler upshift of the laser light reflected off the oscillating plasma surface, acting as a relativistic oscillating mirror (ROM; refs 6,7). The other originates from currents excited by fast electrons in the density ramp of the plasma–vacuum interface leading to what has been dubbed coherent wake emission (CWE; refs 15,17). CWE is dominant at sub- or moderately relativistic intensities[17,18] for $a_L < 1$, whereas ROM becomes more efficient for $a_L > 1$ and completely takes over in the highly relativistic regime[12,19], when $a_L \gg 1$. In the transitional range for $a_L \approx 1$, the two processes can coexist and which one of the two dominates depends sensitively on the shape and gradient of the plasma density profile[18].

Phase coherence of the emitted XUV harmonics necessary for attosecond temporal bunching has been predicted for both generation processes, but the generation mechanisms leading to it have completely different physical origins. CWE is produced by electrons that are first pulled out from the plasma by the electric-field component of the incident laser pulse perpendicular to the target to be hurled back into the plasma during the next half cycle, where they excite plasma oscillations. Through linear mode conversion these plasma oscillations decay into electromagnetic waves at harmonics of the fundamental laser frequency[23]. It is the subfemtosecond temporal confinement of the electrons' re-encounter in the plasma that presumably leads to attosecond pulse formation in this case. The emitted bursts are expected to carry a chirp because their different spectral components are radiated from slightly different depths in the density ramp of the plasma–vacuum interface. On the other hand, ROM harmonics are due to the relativistic Doppler frequency shift acquired by the wave back-reflected from the plasma surface oscillating at velocities close

to the speed of light. Attosecond confinement is expected at the highest emitted frequencies. This is because the maximum Doppler upshift is confined to a small fraction of the laser oscillation period near the instants when the oscillating plasma surface moves towards the impinging laser pulse at maximum velocity. At these moments, the emerging bursts are expected to carry negligible chirp. The superior phase-locking properties of high-order ROM harmonics have been investigated in the theoretical treatment of ref. 12 and verified by wavelet analysis of particle-in-cell simulation results[13]. More details of the harmonic synchronization in connection with the two generation mechanisms, including results of particle-in-cell simulations, are given in Supplementary Information.

To address the question of mutual coherence among XUV harmonics and the resulting attosecond pulse generation from overdense plasmas, we have chosen the method of XUV autocorrelation (AC), which has already been applied successfully to the temporal characterization of atomic harmonic emission[24–26] (for details, see the Methods section). The technique is demanding in itself, but its application to plasma harmonics presents a particularly formidable challenge. This is mainly because, in contrast to the well-collimated XUV beams from atomic harmonic sources, plasma harmonics are emitted in a large cone owing to the tight focusing required for achieving high intensities. Moreover, harmonic generation from solid targets requires an assembly providing an undisturbed surface for each laser shot at a relatively high repetition rate for data accumulation. The experimental set-up shown in Fig. 1 is the result of a compromise between maximum possible collection efficiency and best possible suppression of the fundamental and the harmonics higher than 15th order, both requirements being of critical importance for successful implementation of nonlinear XUV AC. In our experiments we draw on two-photon ionization of He as the nonlinear process, which has been thoroughly investigated previously[27], with the number of $He^+$ ions serving as the physical observable. The approach relies on suppression of harmonics above the 15th order (H15) of the Ti:sapphire driver laser ($\lambda_L = 0.8\,\mu m$) used in our experiments to avoid single-photon ionization of He and on sufficiently intense lower-order harmonics to induce measurable two-photon ionization.

Suppression of harmonics of order $\geqslant 16$ can be ascertained by using a filter with a sharp edge at a photon energy of $\sim$24.6 eV or inhibiting the emission process itself beyond this energy. In our measurements we have exploited both methods to select XUV harmonics between H8 and H14, by filtering with a 150-nm-thick In foil and by confinement of the emission through the generation process to harmonics below the H14. Owing to the In filter, harmonics H8–H10 are the most intense ones in the transmitted spectrum. The harmonics are reproducibly generated by focusing the 45 fs pulses from ATLAS laser system at the Max-Planck-Institut für Quantenoptik (see Methods section) onto a BK7-glass (density $\sim 2.6\ g\,cm^{-3}$) or a polymethylmethacrylate (PMMA) (density $\sim 1.2\ g\,cm^{-3}$) target under 45° angle of incidence (Fig. 1). The spatially averaged, effective laser intensity on target is estimated as $I_L \simeq 4\times10^{18}\ W\,cm^{-2}$, yielding a normalized amplitude of $a_L \simeq 1.5$ for $\lambda_L = 0.8\,\mu m$. At this intensity, both mechanisms discussed above may play a role in the XUV harmonic generation.

However, the appearance of a distinct cut-off in the harmonic emission spectra and the scaling of this cut-off with target density (Fig. 2) suggest that the CWE mechanism provides a dominant contribution in our experiments. In fact, CWE was found to show a well-defined cut-off that moves to higher energy for increasing density[15,18] (see Supplementary Information) as can be seen by comparing the spectra in Fig. 2a,c with those in Fig. 2b,d. The cut-off showing up at H14 for the low-density source corresponds to the maximum resonance frequency that can be supported by the plasma density of this material. This fortuitous circumstance, due mainly to the CWE generation mechanism, is most helpful in suppressing single-photon ionization of the He atoms, which is induced by H16 and higher orders emerging from the high-density source (Fig. 2). As a consequence, we are able to produce a clean two-photon-induced $He^+$ ion signal with the XUV harmonics from the low-density source, as demonstrated by the approximately quadratic scaling of the ion signal with XUV intensity. In clear contrast to this, the ion signal produced with the XUV beam from the high-density source shows a nearly linear intensity scaling, indicating the dominance of single-photon induced transitions in the ionization. Hence the XUV harmonic emission produced from the low-density source and filtered with an In foil (see Fig. 2a) constitutes an ideal prerequisite for the nonlinear AC experiment.

The temporal characterization of the superposition of harmonics shown in Fig. 2a was performed in two steps. The overall duration of the XUV emission is obtained by a coarse scan (delay step size 3.3 fs)

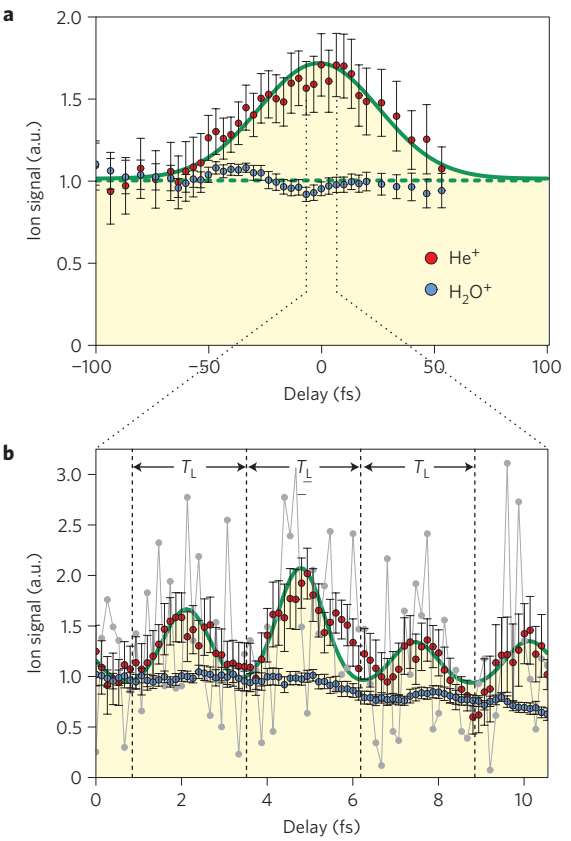


**Figure 3 | Measured nonlinear volume AC of the coherent XUV beam comprising H8–H14 from low-density targets.** The data are obtained from the $He^+$ and $H_2O^+$ ion signal in the mass spectra by varying the delay between the two parts of the split mirror. The moving averages of the raw data taken over nine delay points are shown, with the error bars representing one standard error of the mean. The red circles represent the $He^+$signal produced by two-photon ionization whereas the blue circles the single-photon ionization of $H_2O$. The $H_2O^+$ signal level relative to the $He^+$ signal is scaled arbitrarily. **a**, A coarse scan over the laser pulse duration (delay step 3.3 fs). A Gaussian fit to $He^+$ raw data (green line) yields a duration for the XUV emission $T_{XUV} = 44 \pm 20$ fs. **b**, A fine scan near zero delay with a delay step size of 133 as ($\sim$20 data points per laser cycle). The raw data are shown as grey circles connected by grey lines. The green line is a fit to the raw data (grey circles) of a sequence of Gaussian pulses to the second-order XUV AC signal yielding $\tau_{XUV} = 0.9 \pm 0.4$ fs. In both panels, the $H_2O^+$ signal serves as reference for monitoring the XUV intensity and provides a clear indication of the absence of modulation as a result of single-photon ionization.

of the ion signal as a function of the delay between the two replicas of the XUV pulse prepared by the split mirror for the AC (Fig. 1). From the resultant AC trace shown in Fig. 3a we evaluate an overall duration of the XUV emission as the full-width at half-maximum (FWHM) of the envelope of the XUV emission assuming a Gaussian profile, which gives $T_{XUV} \approx 44 \pm 20$ fs. The fact that this value is very close to the laser pulse duration indicates that CWE scales nearly linearly with laser intensity, which agrees with the findings in ref. 15. To ascertain whether the XUV emission shows a sub-laser-cycle temporal structure indicative of attosecond synchronism among the filtered harmonics, we have performed a fine scan (delay step size 0.13 fs) over a delay interval of ~4 laser cycles centred near the zero delay that yielded the maximum signal in the coarse scan. Figure 3b shows the result of this fine scan. A quasiperiodic subfemtosecond structure with the period of the driving laser field, $T_L$, is clearly discernible. This is in contrast to the time structure of atomic harmonics, which is characterized by a pulse spacing of $T_L/2$ due to the absence of even harmonics in the emission spectrum. Fitting a train of Gaussian pulses to the measured AC trace gives an estimate for the duration of the individual pulses of $\tau_{XUV} \approx 0.9 \pm 0.4$ fs FWHM. This is the first observation of a subfemtosecond pulse train in the emission emanating from a laser–plasma interaction.

The Fourier limit of the pulses that can be synthesized with the filtered harmonic composition is ~0.5 fs. One possible physical reason for the deviation from this value is the existence of chirp. The presence of a chirp in the emitted subfemtosecond bursts is consistent with our previous finding that CWE is the dominant mechanism responsible for XUV emission. As explained in Supplementary Information, the CWE harmonics possess an intrinsic 'atto chirp' and equation (1) predicts for the superposition of the seven harmonics experimentally selected and for estimated plasma scale lengths in the range of $L/\lambda = 0.1$–$0.5$ the emergence of chirped pulses with durations of 0.8–1 fs, in plausible agreement with the experimental data. The accuracy of the measurements however does not allow the definite identification of the source of broadening, and other factors that can contribute to it cannot be excluded. The question concerning the atto chirp of the harmonic emission has to be investigated in more accurate measurements using higher laser intensities. Information thus acquired might reveal superior phase-locking properties associated with the ROM harmonic generation mechanism, as the analysis presented in Supplementary Information presages (see Supplementary Information, Fig. S2).

In summary, our work provides experimental evidence for the phase synchronism of XUV plasma harmonics required for attosecond light bunching. The result motivates advancement of multiterawatt few-cycle laser technology[28], particularly in providing sufficiently high-contrast laser pulses as an alternative to the use of plasma mirrors[16,17]. This will lead to isolated subfemtosecond pulses with peak intensities rivalling those produced by accelerator-based sources[5]. Powerful attosecond pulses from few-cycle-driven overdense plasmas will provide access to correlated intra-atomic electron motion through XUV pump–probe spectroscopy[29] and—with scaling of the laser pulse energy—to unprecedented field strengths[30], holding promise for advancing time-resolved and high-field science likewise.

## Methods

**Experimental set-up.** The ATLAS facility of the Max-Planck-Institut für Quantenoptik, a Ti:sapphire CPA system, has delivered ~700 mJ, 45-fs-FWHM pulses at 10 Hz for the experiments. Its 60-mm-diameter *p*-polarized laser beam was focused by a 30° dielectric-coated optical-quality-polished off-axis parabolic mirror with 160 mm focal length at 45° angle of incidence onto a rotating disc-shaped target (polished BK7-glass or PMMA substrates of 12 cm in diameter) (see Fig. 1). Focusing the beam results in a peak intensity of $\sim 4 \times 10^{19}$ W cm$^{-2}$ on the optical axis, whereas a careful analysis of the experimental record yields a spatially averaged intensity (over the $1/e^2$ radius containing 86% of the energy) of $\sim 4 \times 10^{18}$ W cm$^{-2}$. This average intensity, corresponding to an effective normalized amplitude of $a_L \sim 1.5$, is more pertinent to the experiment because the CWE process is nearly linear in intensity. Third-order AC of the laser pulse yields an intensity contrast of $\sim 10^8$ 4 ps in front of the pulse peak. The disc-shaped targets are mounted on a rotational–translational stage, enabling target-area replenishment with high precision at a rate sufficient for 10 Hz operation. One disc can be exposed to about 5,000 laser shots before replacement.

**Extreme-ultraviolet beam characterization.** The selection of the harmonic composition necessary for XUV AC is accomplished by proper choice of target and thin-film materials. The maximum plasma density available during the interaction with low-density targets (PMMA) is estimated as $n_{e,max}^{\text{low density}}/n_c \approx 200$. This yields a maximum harmonic order of $q_{max}^{\text{low density}} \approx \sqrt{200} \approx 14$. The corresponding cut-off harmonic for high-density (BK7-glass) targets is $q_{max}^{\text{high density}} \approx \sqrt{400} = 20$ because $n_{e,max}^{\text{high-density}}/n_c \approx 400$. Thus, the combination of low-density targets and an In filter results in a harmonic composition consisting of harmonics H8–H14. This ensures sufficient suppression of harmonics higher than H15 that can cause single-photon ionization of He.

The laser-to-XUV conversion efficiency for the spectral range thus selected was estimated by measuring the XUV energy at the split mirror using a calibrated XUV photodiode. Taking into account all losses introduced in the path between the plasma source and the split mirror (recollimating parabolic mirror reflection, $SiO_2$ plate reflection and In filter transmission), which are of the order of $\sim 10^3$, leads to a conservative estimate of $\eta_{XUV} \geqslant 6 \times 10^{-5}$ for the laser-to-XUV conversion efficiency at the source. We have estimated (with the help of ray tracing) the XUV beam diameter at the focus of the split mirror to be about ~10 μm, yielding thus an XUV intensity at the interaction region of $I_{XUV} \simeq (0.5\text{–}1) \times 10^{11}$ W cm$^{-2}$. Also, a detailed study of the focal region similar to the one presented in ref. 25 with variation of the spacing between the two parts of the split mirror has been performed to ascertain the signal-to-background ratio of the volume AC signal under realistic conditions (XUV beam diameter of 25 mm and 8° angle between the incoming and outgoing beams). The relatively large tilt angle introduces some aberrations in the focus, with the consequence that the expected signal-to-background ratio is ~1.5:1 under our experimental conditions. This is in rough agreement with the experimentally observed signal-to-background ratio (see Fig. 3).

**Extreme-ultraviolet AC data acquisition and analysis.** The $He^+$ ion yield was recorded by a time-of-flight mass spectrometer. The ionization occurs through two-XUV-photon non-resonant absorption from all possible combinations of the selected set of harmonics. By piezoelectrically varying the delay between the two halves of the split mirror, the spatial distribution of the XUV intensity in the focal region is changed. Although the total energy remains the same, this intensity variation due to interference of all harmonics for a particular delay allows for second-order AC measurements. For the coarse and fine scans, the mass spectra were obtained by accumulating 20 shots at each delay value and taking their average. The mass spectra thus recorded were stored for further analysis in an array of ~80 delay steps, representing approximately 1600 shots in the fine scan.

The $He^+$ signal in the coarse as well as in the fine scan represents the second-order AC of the two delayed XUV pulses. To make the trend of AC clearer, the moving averages of the raw data are taken over nine delay points and shown in Fig. 3 with the error bars representing one standard error to the mean. For the case of the coarse scan, a Gaussian fit to $He^+$ raw data (green line) yields the overall duration of the XUV emission $T_{XUV} = 44 \pm 20$ fs FWHM. For the $H_2O^+$ a straight line fit is used (green dashed line). In the case of the fine scan, a fit to the raw data (grey points) of five Gaussians with background was performed (green line). The constraints imposed on the fit were that (1) the interval between the peaks was kept equal to the laser period, 2.67 fs, and (2) all five Gaussians have the same but variable width. The other parameters such as amplitude of each peak and background level were free to vary. This gives an estimate for the subfemtosecond pulse duration as $\tau_{XUV} \approx 0.9 \pm 0.4$ fs FWHM.

The effect of the smoothing over nine delay points (red and blue circles) on the AC signal duration $\tau_0$ (FWHM) can be estimated using the expression $\tau_1^2 \approx \tau_0^2 + \tau_F^2$ (strictly valid for the convolution of two Gaussians), where $\tau_F$ is the width of the smoothing function and $\tau_1$ the resulting width after smoothing. (The XUV pulse durations have been estimated from the AC signal durations using the approximation $\tau_{XUV} \approx \tau_0/\sqrt{2}$.) In the case of the coarse scan for $\tau_0 \approx 62.2$ fs (deduced from the fit to the raw data) and $\tau_F \approx 8 \times 3.3 = 26.4$ fs we obtain $\tau_1 \approx 67.6$ fs. This represents less than 10% difference, and as consequence the fitted curve and the smoothed signal are almost indistinguishable. The corresponding values for the case of the fine scan are $\tau_0 \approx 1.3$ fs (again deduced from the fit to the raw data) and $\tau_F \approx 8 \times 0.13 = 1.04$ fs, thus $\tau_1 \approx 1.7$ fs. Here the effect is larger (about 30%), but given the large error bars associated with the smoothed data the difference between the fitted curve and the smoothed data is barely discernible. For the same reason, the change in the signal-to-background ratio after smoothing is not substantially affected.

Received 6 June 2008; accepted 10 November 2008; published online 14 December 2008

## References


1. Goulielmakis, E. *et al.* Single-cycle nonlinear optics. *Science* **320**, 1614–1617 (2008).
2. Sansone, G. *et al.* Isolated single-cycle attosecond pulses. *Science* **314**, 443–446 (2006).
3. Drescher, M. *et al.* Time-resolved atomic inner-shell spectroscopy. *Nature* **419**, 803–807 (2002).
4. Cavalieri, A. L. *et al.* Attosecond spectroscopy in condensed matter. *Nature* **449**, 1029–1032 (2007).
5. Ackermann, W. *et al.* Operation of a free-electron laser from the extreme ultraviolet to the water window. *Nature Photon.* **1**, 336–342 (2007).
6. Bulanov, S. V., Naumova, N. M. & Pegoraro, F. Interaction of an ultrashort, relativistically strong laser pulse with an overdense plasma. *Phys. Plasmas* **1**, 745–757 (1994).
7. Lichters, R., Meyer-ter-Vehn, J. & Pukhov, A. Short-pulse laser harmonics from oscillating plasma surfaces driven at relativistic intensity. *Phys. Plasmas* **3**, 3425–3437 (1996).
8. Plaja, L., Roso, L., Rzążewski, K. & Lewenstein, M. Generation of attosecond pulse trains during the reflection of a very intense laser on a solid surface. *J. Opt. Soc. Am. B* **15**, 1904–1911 (1998).
9. Naumova, N. M., Nees, J. A., Sokolov, I. V., Hou, B. & Mourou, G. A. Relativistic generation of isolated attosecond pulses in a $\lambda^3$ focal volume. *Phys. Rev. Lett.* **92**, 063902 (2004).
10. Gordienko, S., Pukhov, A., Shorokhov, O. & Baeva, T. Relativistic Doppler effect: Universal spectra and zeptosecond pulses. *Phys. Rev. Lett.* **93**, 115002 (2004).
11. Tsakiris, G. D., Eidmann, K., Meyer-ter-Vehn, J. & Krausz, F. Route to intense single attosecond pulses. *New J. Phys.* **8**, 19 (2006).
12. Baeva, T., Gordienko, S. & Pukhov, A. Theory of high-order harmonic generation in relativistic laser interaction with overdense plasma. *Phys. Rev. E* **74**, 046404 (2006).
13. Rykovanov, S. G., Geissler, M., Meyer-ter-Vehn, J. & Tsakiris, G. D. Intense single attosecond pulses from surface harmonics using the polarization gating technique. *New J. Phys.* **10**, 025025 (2008).
14. Tarasevitch, A. *et al.* Generation of high-order spatially coherent harmonics from solid targets by femtosecond laser pulses. *Phys. Rev. A* **62**, 023816 (2000).
15. Quéré, F. *et al.* Coherent wake emission of high-order harmonics from overdense plasmas. *Phys. Rev. Lett.* **96**, 125004 (2006).
16. Dromey, B. *et al.* High harmonic generation in the relativistic limit. *Nature Phys.* **2**, 456–459 (2006).
17. Thaury, C. *et al.* Plasma mirrors for ultrahigh-intensity optics. *Nature Phys.* **3**, 424–429 (2007).
18. Tarasevitch, A., Lobov, K., Wünsche, C. & von der Linde, D. Transition to the relativistic regime in high order harmonic generation. *Phys. Rev. Lett.* **98**, 103902 (2007).
19. Dromey, B. *et al.* Bright multi-keV harmonic generation from relativistically oscillating plasma surfaces. *Phys. Rev. Lett.* **99**, 085001 (2007).
20. Farkas, Gy. & Tóth, Cs. Proposal for attosecond light pulse generation using laser induced multiple-harmonic conversion processes in rare gases. *Phys. Lett. A* **168**, 447–450 (1992).
21. Agostini, P. & DiMauro, L. F. The physics of attosecond light pulses. *Rep. Prog. Phys.* **67**, 813–855 (2004).
22. Quéré, F. *et al.* Phase properties of laser high-order harmonics generated on plasma mirrors. *Phys. Rev. Lett.* **100**, 095004 (2008).
23. Hinkel-Lipsker, D. E., Fried, B. D. & Morales, G. J. Analytic expression for mode conversion of Langmuir and electromagnetic waves. *Phys. Rev. Lett.* **62**, 2680–2682 (1989).
24. Kobayashi, Y., Sekikawa, T., Nabekawa, Y. & Watanabe, S. 27-fs extreme ultraviolet pulse generation by high-order harmonics. *Opt. Lett.* **23**, 64–66 (1998).
25. Tzallas, P., Charalambidis, D., Papadogiannis, N. A., Witte, K. & Tsakiris, G. D. Direct observation of attosecond light bunching. *Nature* **426**, 267–271 (2003).
26. Nabekawa, Y. *et al.* Conclusive evidence of an attosecond pulse train observed with the mode-resolved autocorrelation technique. *Phys. Rev. Lett.* **96**, 083901 (2006).
27. Nikolopoulos, L. A. A. *et al.* Second order autocorrelation of an XUV attosecond pulse train. *Phys. Rev. Lett.* **94**, 113905 (2005).
28. Tavella, F. *et al.* Dispersion management for a sub-10-fs, 10 TW optical parametric chirped-pulse amplifier. *Opt. Lett.* **32**, 2227–2229 (2007).
29. Hu, S. X. & Collins, L. A. Attosecond pump probe: Exploring ultrafast electron motion inside an atom. *Phys. Rev. Lett.* **96**, 073004 (2006).
30. Gordienko, S., Pukhov, A., Shorokhov, O. & Baeva, T. Coherent focusing of high harmonics: A new way towards the extreme intensities. *Phys. Rev. Lett.* **94**, 103903 (2005).


## Acknowledgements

This work was supported in part by DFG-Project Transregio TR18, by The Munich Centre for Advanced Photonics (MAP), by the European Community's Human Potential Programme under contract MRTN-CT-2003-505138 (XTRA) and MTKD-CT-2004-517145 (X-HOMES), by the FP6 project 'Laserlab-Europe', contract RII3-CT-2003-506350, and by the Association EURATOM—Max-Planck-Institut für Plasmaphysik.

## Additional information

Supplementary Information accompanies this paper on www.nature.com/naturephysics. Reprints and permissions information is available online at http://npg.nature.com/reprintsandpermissions. Correspondence and requests for materials should be addressed to G.D.T.